Article

Artificial Neural Network Models for Determining the Load-Bearing Capacity of Eccentrically Compressed Short Concrete-Filled Steel Tubular Columns

Anton Chepurnenko [1,*] **, Vasilina Turina** [1] **and Vladimir Akopyan** [2]

1 Structural Mechanics and Theory of Structures Department, Don State Technical University, 344003 Rostov-on-Don, Russia; vasilina.93@mail.ru
2 Engineering Geology, Bases and Foundations Department, Don State Technical University, 344003 Rostov-on-Don, Russia; vovaakop@mail.ru
* Correspondence: anton_chepurnenk@mail.ru; Tel.: +7-863-201-9136

Abstract: Artificial neural networks (ANN) have a great promise in predicting the load-bearing capacity of building structures. The purpose of this work was to develop ANN models to determine the ultimate load of eccentrically compressed concrete-filled steel tubular (CFST) columns of circular cross-sections, which operated on the widest possible range of input parameters. Short columns were considered for which the amount of deflection does not affect the bending moment. A feedforward network was selected as the neural network type. The input parameters of the neural networks were the outer diameter of the columns, the thickness of the pipe wall, the yield strength of steel, the compressive strength of concrete and the relative eccentricity. Artificial neural networks were trained on synthetic data generated based on a theoretical model of the limit equilibrium of CFST columns. Two ANN models were created. When training the first model, the ultimate loads were determined at a given eccentricity of the axial force without taking into account additional random eccentricity. When training the second model, additional random eccentricity was taken into account. The total volume of the training dataset was 179,025 samples. Such a large training dataset size has never been used before. The training dataset covers a wide range of changes in the characteristics of the pipe metal and concrete of the core, pipe diameters and wall thicknesses, as well as eccentricities of the axial force. The trained models are characterized by high mean square error (MSE) scores. The correlation coefficients between the predicted and target values are very close to 1. The ANN models were tested on experimental data for 81 eccentrically compressed samples presented in five different works and 265 centrally compressed samples presented in twenty-six papers.

Keywords: concrete-filled steel tubular columns; load bearing capacity; ultimate equilibrium; artificial neural networks; machine learning

1. Introduction

Concrete-filled steel tubular columns are a promising type of building structure. They are widely used in the construction of high-rise buildings, transport structures, overpasses, etc. [1–4]. Compared to traditional reinforced concrete elements, CFST structures have a number of advantages, which primarily include an increase in load-bearing capacity due to the work of concrete under conditions of triaxial compression [5], savings on formwork and reinforcement work, etc.

Improving methods for calculating the load-bearing capacity of CFST columns is an urgent task, which is confirmed by the large number of theoretical and experimental works published recently on this topic [6–8].

When determining the load-bearing capacity of CFST columns, two approaches are most common. The first approach is to use empirical dependencies obtained from experimental data [9]. These dependencies are quite simple and suitable for engineering

calculations, but the range of parameter changes in which the experiments were carried out limits their scope.

The second approach is finite element modeling in a three-dimensional setting, taking into account the real deformation diagrams of concrete and steel, as well as the contact interaction between the shell and the concrete core. A significant number of publications are devoted to the issues of finite element modeling of the stress–strain state of CFST columns [10–17]. This approach provides good agreement with experimental data but requires great computational resources and time.

Recently, machine learning methods have been widely used in the task of predicting the load-bearing capacity of CFST columns. In the work by Tran et al. [18], an empirical formula was proposed to determine the load-bearing capacity of centrally compressed square-section concrete tubular columns using an artificial neural network (ANN). ANN training was performed on experimental data for 300 columns presented in the literature. A comparative analysis showed greater stability and accuracy of the ANN compared to other existing formulas.

In another work, Tran et al. [19] built an artificial neural network model to predict the load-bearing capacity of centrally compressed CFST columns with a circular cross-section. Unlike the previous work, training was carried out on the results of numerical experiments rather than full-scale ones. To generate the dataset, three-dimensional finite element analysis was used in a nonlinear formulation in the ABAQUS environment. The ANN training database included data for 768 columns with different lengths, outer cross-sectional diameters, pipe wall thickness, steel yield strength and concrete compressive strength. For practical engineering calculations, the authors prepared a tool with a graphical interface.

In ref. [20], Du et al. proposed two ANN models to determine the ultimate load under central compression of square-section CFST columns. Both models were trained on experimental data for 275 samples, and 30 samples were used for testing. The output data of the neural networks was compared with the results of calculations according to the design codes of various countries, and it was found that the resulting functional dependence of the load-bearing capacity on the main parameters differs somewhat from those presented in the design codes.

In ref. [21], Al-Khaleefi et al. discussed the issues of predicting the fire resistance of CFST columns using artificial neural networks. Based on neural network modeling, a functional dependence of the CFST columns' fire resistance index on the parameters that determine the dimensions of the samples, material characteristics and loading conditions was constructed. The total dataset included 35 experimental samples, of which 27 samples were used for training and 8 for testing. Another study on predicting the fire resistance of CFST columns using an ANN is presented in the work of Moradi et al. [22]. This paper is based on a larger database, including testing of 300 samples.

In ref. [23], Zarringol et al. built artificial neural network models to predict the ultimate load for CFST columns of rectangular and circular cross-sections under central and eccentric compression. Compared to the previous works, larger datasets were used to train the ANN: 895 experiments for centrally compressed rectangular columns, 392 experiments for eccentrically compressed rectangular columns, 1305 experiments for centrally compressed circular columns, and 499 experiments for circular columns subjected to eccentric compression. The accuracy of ultimate load prediction was also compared with design codes of various countries.

CFST columns are also the object of study of ref [24], in which the ultimate load under central compression of columns was predicted using Multiphysics Artificial Intelligence. This article compared models based on an artificial neural network, Adaptive Neuro-Fuzzy Inference System (ANFIS), and Gene Expression Programming (GEP). The research dataset contained data from 1667 experiments, of which 702 corresponded to short columns and 965 corresponded to long columns. Gene Expression Programming, in combination with the finite element method, was also used in [25] to predict the strength of CFST columns made of high-strength concrete.

Ref [26] proposes a hybrid model that includes an ANN with a particle swarm optimization (PSO) algorithm. This model was used to predict flexural bending capacity and flexural stiffness at the initial and serviceability limits of CFST beams.

Among recent artificial intelligence techniques, the gradient boosting algorithm is currently gaining great popularity. Ref [27] demonstrates the application of this algorithm to predicting the strength of centrally compressed CFST columns of circular cross-sections. A comparison was made with other machine learning algorithms, such as random forest (RF), support vector machines (SVM), decision tree (DT) and deep learning.

In ref. [28], the following machine learning models were applied to solve the same problem: back-propagation neural network (BPNN), genetic algorithm (GA)-BPNN, radial basis function neural network (RBFNN), Gaussian process regression (GPR) and multiple linear regression (MLR). The training dataset included 2045 centrally compressed columns selected through an extensive literature review. This paper shows that forecasting efficiency can be improved by dividing columns into subgroups depending on slenderness.

There are also publications in which machine learning methods are used not only to predict the ultimate load but also to predict the load–strain curve. In ref. [29], Zarringol et al. showed the successful use of an artificial neural network in engineering calculations, which predicts the complete deformation diagram of centrally compressed CFST columns of round and square sections. For training, a database was used that included the results of 1152 finite element calculations in the ABAQUS environment, as well as the results of 392 full-scale experiments.

The review shows that machine learning methods are a promising tool in predicting the load-bearing capacity of CFST columns. At the same time, most existing publications refer to centrally compressed elements. For eccentrically compressed columns, compared to centrally compressed structures, an additional parameter affecting the load-bearing capacity is the eccentricity of the axial force. Therefore, to build ANN models that predict the load-bearing capacity of eccentrically compressed CFST columns, a significantly larger dataset size is required. The purpose of this work is to develop artificial neural network models that could predict with high accuracy the ultimate load for the entire possible range of parameters affecting the load-bearing capacity of eccentrically compressed columns. In our case, neural networks will be trained on synthetic data obtained on the basis of a theoretical model, followed by comparison with experimental data.

2. Materials and Methods

The process of building a model of any artificial neural network includes choosing its architecture and training. As an environment for implementing the ANN model, the MATLAB package (Neural Network Toolbox) was selected.

The CFST columns of circular cross-sections were selected as the object of study since this cross-sectional shape is the most common in the designs of buildings and structures for various purposes. The prediction of the ultimate load N_{ult} (kN) in the developed ANN models was carried out according to 5 input parameters: outer diameter of the column D_p (mm), pipe wall thickness t_p (mm), yield strength of steel R_y (MPa), compressive strength of concrete R_b (MPa) and relative eccentricity e/D_p. We were considering short columns for which deflection did not lead to a significant increase in the bending moment, so the length of the elements was not included in the input parameters. Columns, according to [30], are considered short if their slenderness (the ratio of the calculated length to the radius of gyration of the section) does not exceed 14.

A feedforward network architecture was selected as it is one of the most common neural network types. The developed ANN model contains 2 hidden layers. The number of neurons in each hidden layer is 16. The TANSIG (hyperbolic tangent) function was used as the activation function for neurons in both layers. The architecture of the developed neural networks is shown schematically in Figure 1.
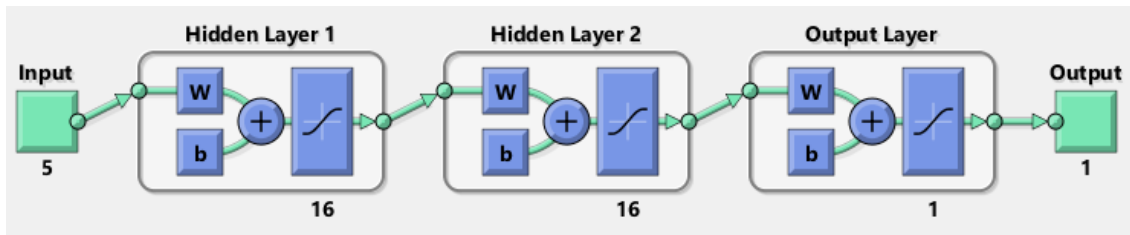
Figure 1. Artificial neural network architecture.

Unlike most previous works, where training is carried out on experimental data, in our work the neural networks were trained on synthetic data. Experimental data were not used for training, since they are not so numerous and could not cover the full variety of column sizes and concrete and steel characteristics. However, after training the neural networks, their performance was tested using experimental data.

When generating a dataset for training, the provisions presented in the Russian design codes for composite steel and concrete structures SR 266.1325800.2016 [30] were used. Columns without bar reinforcement were considered, in which only a steel pipe acts as a reinforcement. When determining the breaking load, the stress diagrams in concrete and steel in the limit state were assumed to be rectangular; the work of tensile concrete was not taken into account. The diagram for determining the ultimate load under eccentric compression of a CFST column is shown in Figure 2.
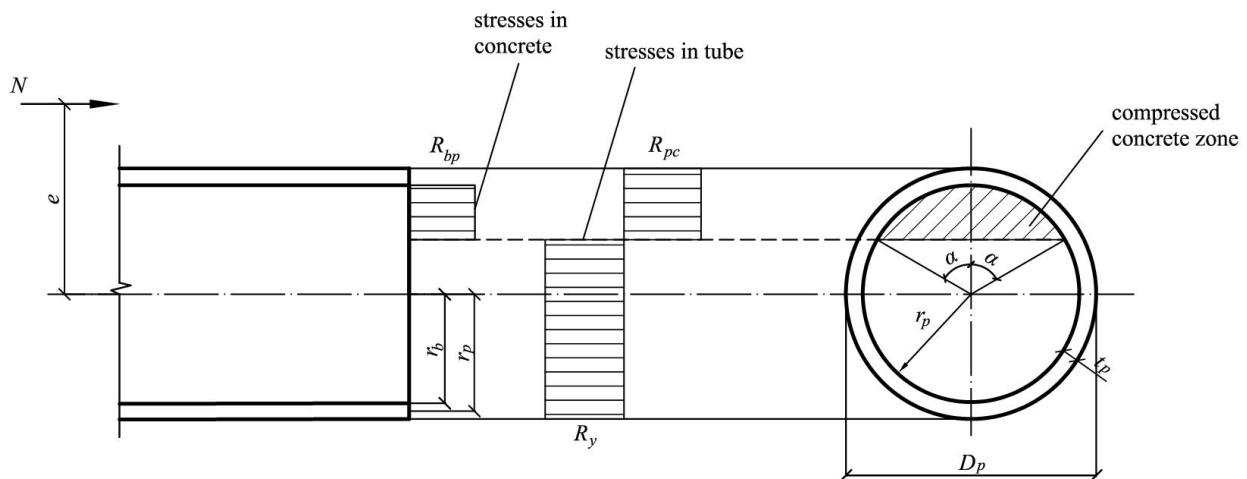
Figure 2. Diagram for determining the ultimate load.

The strength calculation of normal sections of eccentrically compressed CFST elements without bar reinforcement according to SR 266.1325800.2016 is performed by the limit equilibrium method from the condition:

$$N \cdot e \leq \frac{2}{3} r_b^3 R_{bp} \sin^3 \alpha + \frac{1}{\pi} A_p r_p \sin \alpha \left(R_y + R_{pc} \right), \tag{1}$$

where N is the axial force, e is the eccentricity of the axial force, $r_b = \left(D_p - 2t_p \right)/2$ is the radius of the concrete core, R_{bp} is the compressive design strength of concrete taking into account the effect of lateral compression, α is the angle that determines the size of the compressed zone of concrete, $A_p = \pi D_p t_p$ is the cross-sectional area of the steel pipe, $r_p = \left(D_p - t_p \right)/2$ is the average radius of the steel pipe, R_{pc} is the design strength of a steel pipe under compression.

The compressive design strength of concrete taking into account the effect of lateral compression in [30] is determined by the formula:

$$R_{bp} = R_b + \Delta R_b \cdot m;$$

$$\Delta R_b = \left(2 + 2.52 \cdot e^{-\frac{1}{c}(R_y A_p + R_b A_b)}\right) \frac{t_p}{D_p - 2t_p} R_p;$$

$$m = \begin{cases} 1 - \frac{7.5e}{D_p - 2t_p}, & if\ D_p - 2t_p - 7.5e \geq 0 \\ 0, & if\ D_p - 2t_p - 7.5e < 0 \end{cases}.$$

(2)

The coefficient c in Formula (2) is taken equal to 25 MN.

The design strength of a pipe under compression is determined by the formula:

$$R_{pc} = R_y(1 - 0.25 \cdot m).$$

(3)

Angle α in Formula (1) is determined from the equation:

$$r_b^2 \left(\alpha - \frac{1}{2}\sin 2\alpha\right) R_{bp} + \frac{\alpha}{\pi} A_p R_{pc} - \left(1 - \frac{\alpha}{\pi}\right) A_p R_y = N.$$

(4)

Expression (1) allows one to check the fulfillment of the column strength condition but does not find the ultimate load at a given eccentricity. For a given eccentricity of the axial force e, determining the magnitude of the ultimate load based on the SR 266.1325800.2016 method is a very non-trivial task. Equation (4) is transcendental and requires the use of numerical methods to solve. The task of determining the ultimate compressive force at a known value of e was solved by us by stepwise increasing the load from 0 to $N_{ult,0}$, where $N_{ult,0}$ is the ultimate load for a given sample under central compression. At each step, the root of Equation (4) was numerically determined, and then the fulfillment of Condition (1) was checked. When generating the training sample, the range of changes in the compressive strength of concrete R_b was taken from 10 to 65 MPa; the yield strength of the steel varied from 240 to 440 MPa. The relative eccentricity e/D_p varied from 0 to 0.65. The values of outer diameters of pipes and wall thicknesses used during training corresponded to the Russian assortment of electric-welded straight-seam pipes GOST 10704-91 (Table 1).

For quantities R_b and R_y, 5 different values were used from $R_{b,min}$ ($R_{y,min}$) to $R_{b,max}$ ($R_{y,max}$) with uniform steps. For wall thickness t_p, 11 different values from $t_{p,min}$ to $t_{p,max}$ were used in uniform increments. For the relative eccentricity, 21 different values e/D_p were taken from 0 to 0.65 with equal steps. Thus, the size of the training sample was $5 \times 5 \times 11 \times 21 \times 31 = 179,025$.

During training, the sample was randomly divided into 3 parts: "Train", "Validation" and "Test" in the proportion of 70%, 15% and 15%. To train the ANN, we used the Levenberg–Marquardt algorithm. The value of the mean square error (MSE) was taken as a criterion for the quality of training:

$$\text{MSE} = \frac{1}{n_s}\sum_{i=1}^{n_s}(d_i - y_i)^2,$$

(5)

where n_s is the sample size, y_i are the target values and d_i are the predicted values.

Table 1. The values of the outer diameters of pipes, as well as the minimum and maximum wall thicknesses used in training.

№	D_p,mm	t_p,mm	
		Min	Max
1	102	1.8	5.5
2	108	1.8	5.5
3	114	1.8	5.5
4	127	1.8	5.5
5	133	1.8	5.5
6	140	1.8	5.5
7	152	1.8	5.5
8	159	1.8	8
9	168	1.8	8

Table 1. *Cont.*

№	D_p,mm	t_p,mm	
		Min	Max
10	177.8	1.8	8
11	180	4	5
12	193.7	2	8
13	219	2.5	22
14	244.5	3	22
15	273	3.5	22
16	325	4	22
17	355.6	4	22
18	377	4	22
19	406.4	4	22
20	426	4	22
21	478	5	12
22	508	4.5	24
23	530	5	20
24	630	7	24
25	720	7	30
26	820	7	30
27	920	7	20
28	1020	8	32
29	1120	8	20
30	1220	9	32
31	1420	10	32

In addition to the ANN model trained to determine the maximum load at a given eccentricity value e, another ANN model was also built to determine the value N_{ult}, taking into account additional random eccentricity. In accordance with Russian standards for the design of composite steel and concrete structures [30], the largest of the values [0.01 m; $D_p/30$; $l/600$] was taken as a random eccentricity, where l was the design length of the column. Since short columns were considered, the value of random eccentricity was taken as the largest of the two values [0.01 m; $D_p/30$].

3. Results and Discussion

Figure 3 shows the training performance graph for the model trained on ultimate loads without taking into account additional random eccentricities. Figure 4 is the same for the model trained taking into account additional random eccentricities. In the first case, the learning process took 474 epochs, and in the second case, it took 682 epochs. The model trained without taking into account additional random eccentricities is characterized by a four-times-smaller MSE value: 4693 vs. 18,940. The MSE values for the "Train", "Validation" and "Test" parts of the sample are almost the same: the blue, green and red lines overlap each other. A small difference in MSE for the "Train", "Validation" and "Test" parts of the sample indicates its sufficient volume.

Figures 5 and 6 show regression plots for the two models. The x-axis shows the target values T of the ultimate load. The y-axis shows the predicted Y values of the ultimate load. Most of the points on the graphs fit on the straight line Y = T. The correlation coefficients R of both models are close to 1. High correlation coefficients between the target and predicted values are achieved thanks to the two-layer neural network architecture, large number of neurons in hidden layers and large dataset size.
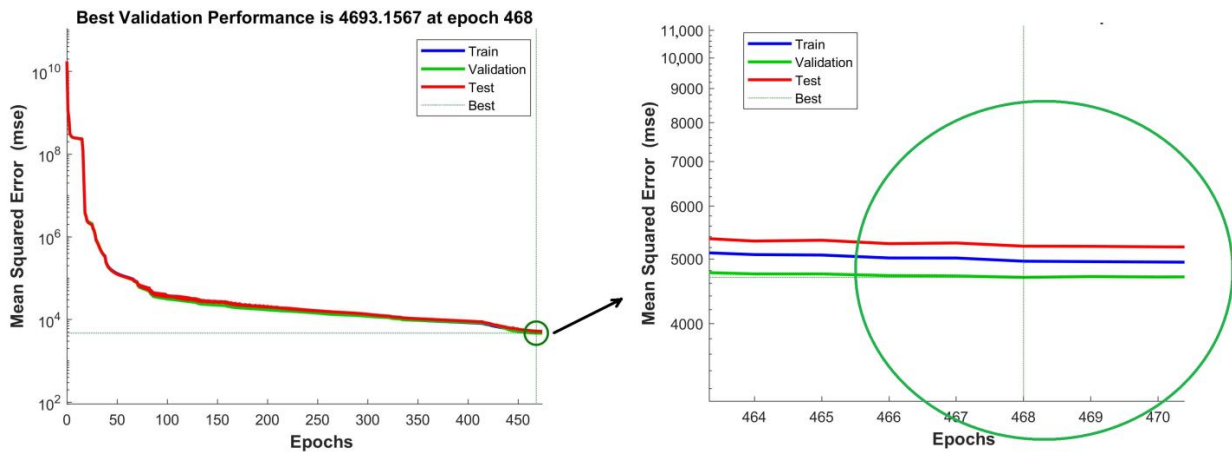
Figure 3. Training performance graph for the model trained without taking into account random eccentricities.
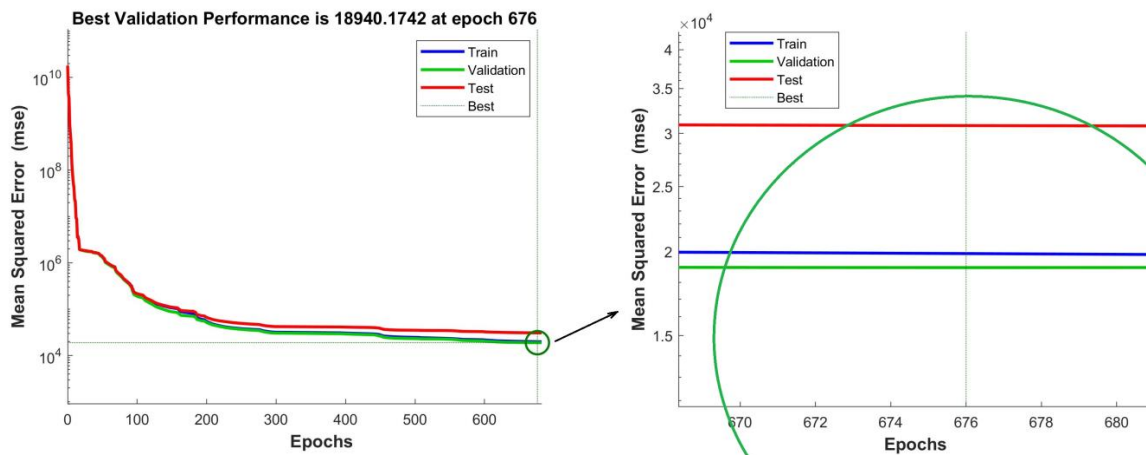
Figure 4. Training performance plot for the model trained with additional random eccentricities.

The constructed models were tested on experimental data for 81 eccentrically compressed CFST columns of circular cross-sections, presented in five different works [31–35]. The diameter of the columns varied from 103 to 720 mm. The wall thickness changed from 1.81 to 11.95 mm. The yield strength of steel varied from 248.9 to 440 MPa. The compressive strength of concrete changed from 21.5 to 63.8 Mpa. The ratio of the axial force eccentricity to the outer diameter of the column e/D_p varied from 0.05 to 0.64. The results are summarized in Table 2. In this table, N_1 are the values of the ultimate loads determined by the first ANN model (without taking into account additional random eccentricities), and N_2 are the values of the ultimate loads determined by the second ANN model (taking into account additional random eccentricities).

From Table 2, it can be seen that for most samples the results predicted by the first model are in good agreement with the experimental data. The average value of the ratio N_1/N_{exp} is 0.97, maximum value is 1.38 and minimum value is 0.79. The standard deviation $\sigma = 0.11$ and the coefficient of variation CV = 10.9%.

Deviations of the predicted values from the experimental results can be explained, on the one hand, by the scatter of experimental data and, on the other hand, by simplifications adopted in the theoretical model, which is used to train the artificial neural network. It should also be noted that, at present, there is no generally accepted criterion for CFST columns to reach the limit state. Some researchers take the magnitude of deformation as a criterion for destruction and others take the achievement of the pipe material's yield point, etc.
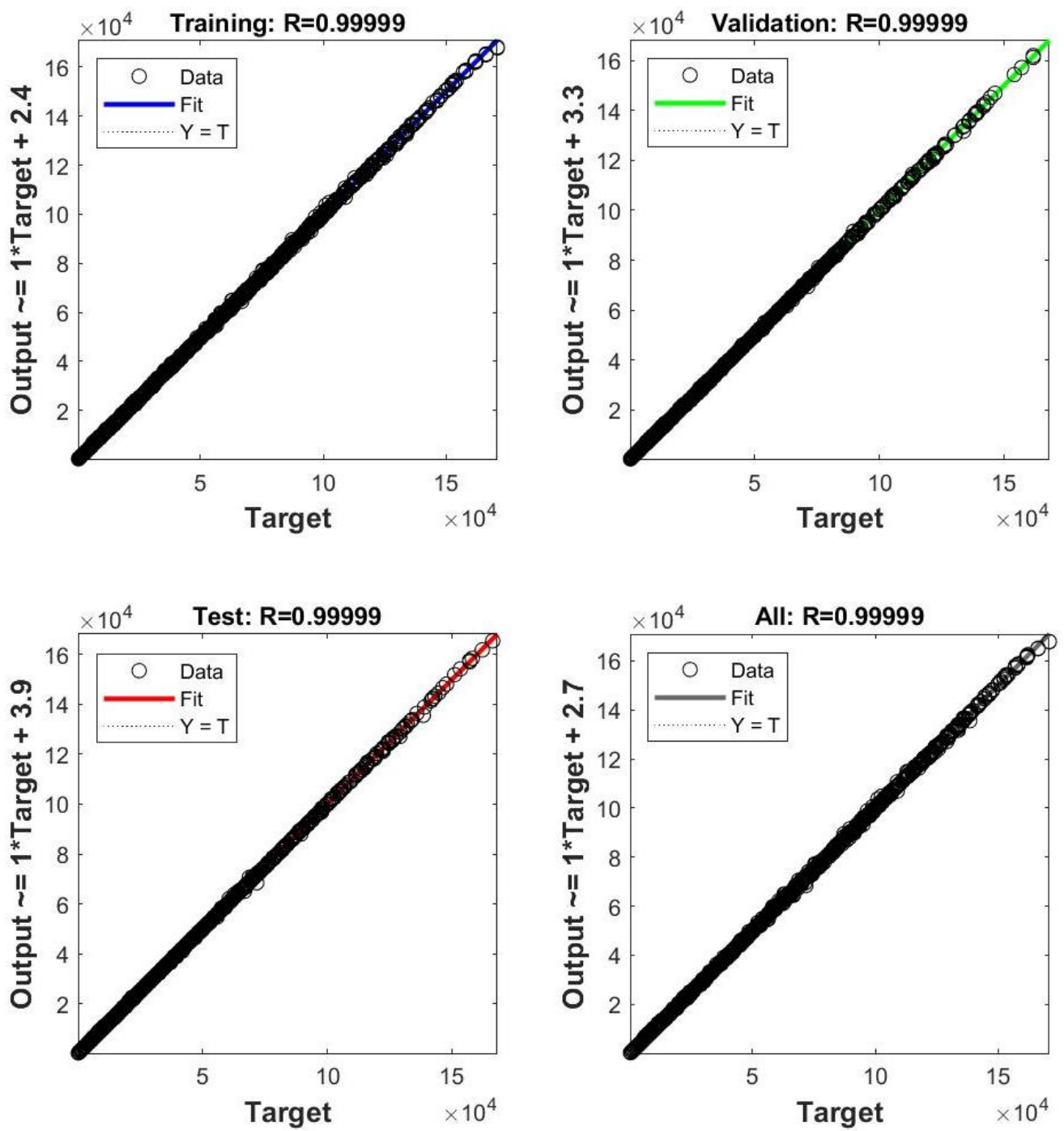
Figure 5. Regression plot for the model trained without taking into account additional random eccentricities.
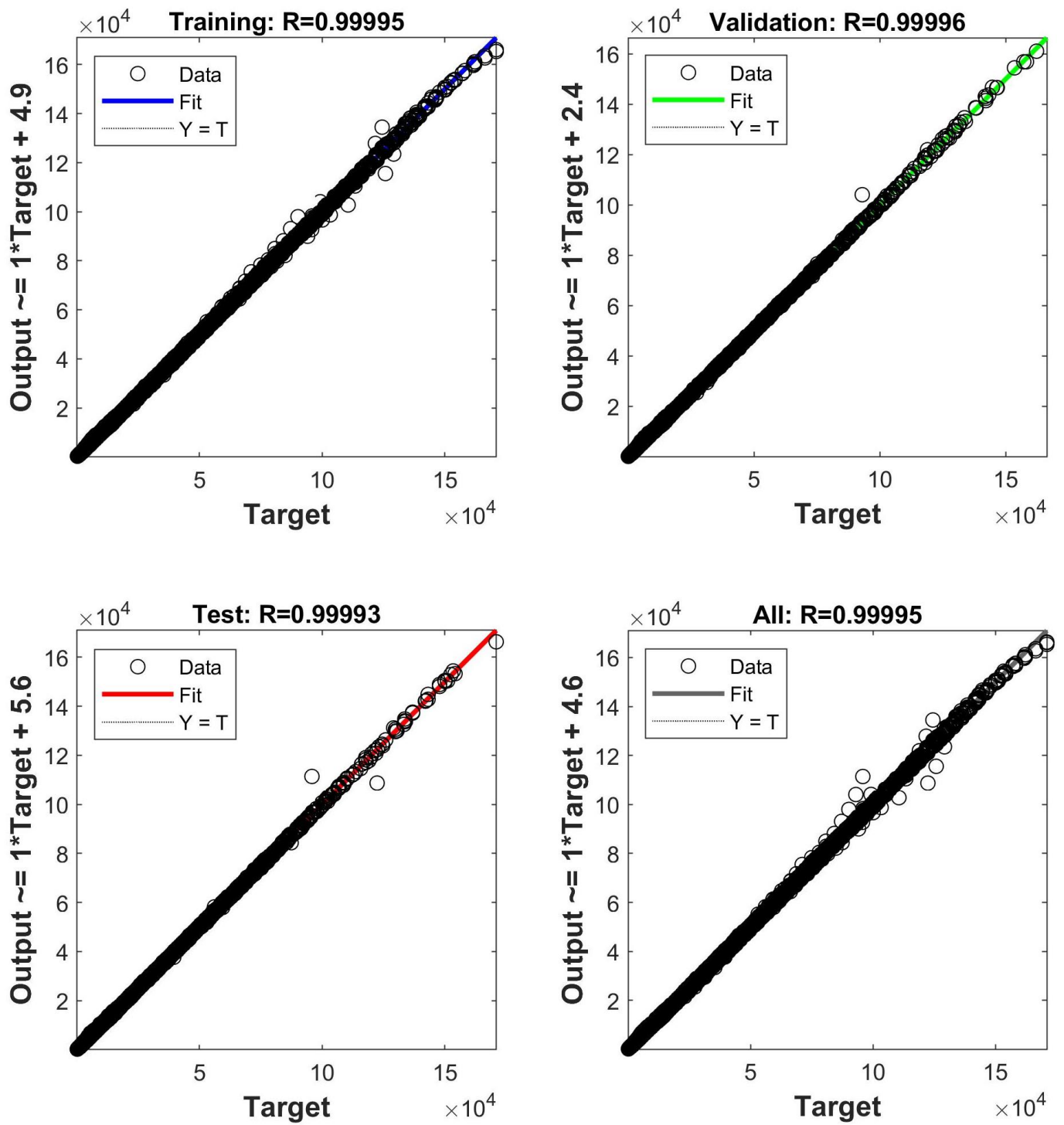
Figure 6. Regression plot for a model trained taking into account additional random eccentricities.

Table 2. Results of testing the developed models of artificial neural networks on experimental data for eccentrically compressed CFST columns.

№	Experiment	e/D_p	D_p, mm	t_p, mm	R_y, MPa	R_b, MPa	N_{exp}, kN	N_1, kN	$\frac{N_1}{N_{exp}}$	N_2, kN	$\frac{N_2}{N_{exp}}$
					Luksha and Nesterovich [31]						
1	SB1	0.06	159	6	295	24.4	1406	1475	1.05	1044	0.74
2	SB2	0.13	159	6	295	25	1210	1045	0.86	850	0.70
3	SB3	0.26	159	6	295	26.9	932	831	0.89	700	0.75
4	SB4	0.06	159	6	295	35.7	1559	1659	1.06	1228	0.79
5	SB5	0.13	159	6	295	36.4	1412	1194	0.85	975	0.69
6	SB6	0.26	159	6	295	39	1066	936	0.88	797	0.75
7	SB7	0.06	219	8	290	36.1	2921	3084	1.06	2348	0.80
8	SB8	0.13	219	8	290	33.9	2698	2141	0.79	1841	0.68
9	SB9	0.26	219	8	290	35.7	1962	1667	0.85	1495	0.76
10	SB10	0.06	219	8	290	51.2	3308	3570	1.08	2797	0.85
11	SB11	0.13	219	8	290	48.2	3041	2498	0.82	2140	0.70
12	SB12	0.26	219	8	290	50.7	2289	1922	0.84	1719	0.75
13	SB13	0.13	159	6	440	43.2	1774	1624	0.92	1393	0.79
14	SB14	0.25	159	6	440	46.2	1346	1315	0.98	1144	0.85
15	SB15	0.38	159	6	440	42.2	1059	1004	0.95	888	0.84
16	SB16	0.13	159	6	440	60.3	1842	1890	1.03	1565	0.85
17	SB17	0.25	159	6	440	62.2	1515	1486	0.98	1269	0.84
18	SB18	0.38	159	6	440	63.8	1238	1162	0.94	1011	0.82
19	SB19	0.13	106	4	435	45	849	771	0.91	638	0.75
20	SB20	0.25	106	4	435	45.8	633	623	0.98	521	0.82
21	SB21	0.38	106	4	435	41.6	468	472	1.01	409	0.87
22	SB22	0.13	106	4	435	59	839	888	1.06	698	0.83
23	SB23	0.25	106	4	435	62.9	691	725	1.05	581	0.84
24	SB24	0.38	106	4	435	62.5	572	557	0.97	464	0.81
25	SB25	0.06	530	7.8	349.2	38.3	12,500	13,604	1.09	13,163	1.05
26	SB26	0.12	530	7.8	349.2	38.3	10,700	10,600	0.99	9227	0.86
27	SB27	0.06	530	11.95	322.6	38.3	14,500	15,636	1.08	15,350	1.06
28	SB28	0.12	530	11.95	322.6	38.3	12,500	11,519	0.92	10,636	0.85
29	SB29	0.06	630	6.6	303	28.4	12,000	13,351	1.11	12,977	1.08
30	SB30	0.13	630	6.6	303	28.4	10,500	9857	0.94	8877	0.85
31	SB31	0.06	630	9.8	311	38.8	17,000	18,821	1.11	18,655	1.10
32	SB32	0.13	630	9.8	311	38.8	15,000	13,189	0.88	12,613	0.84
33	SB33	0.06	720	7.7	395.4	31.4	18,500	20,793	1.12	20,405	1.10
34	SB34	0.13	720	7.7	395.4	31.4	16,000	15,096	0.94	13,589	0.85
35	SB35	0.06	720	9.6	315.6	31.4	18,500	20,587	1.11	20,504	1.11
36	SB36	0.13	720	9.6	315.6	31.4	16,000	14,660	0.92	13,751	0.86
37	SB37	0.06	720	11.74	274	31.4	19,000	20,943	1.10	20,377	1.07
38	SB38	0.13	720	11.74	274	31.4	16,650	14,649	0.88	13,765	0.83
					Matsui et al. [32]						
39	4-21	0.13	165.2	4.17	358.7	40.9	1265	1190	0.94	1053	0.83
40	4-63	0.38	165.2	4.17	358.7	40.9	767	726	0.95	661	0.86
41	4-105	0.64	165.2	4.17	358.7	40.9	558	482	0.86	447	0.80
42	P-78-2	0.07	106	3	298.9	37.1	603	639	1.06	441	0.73
43	P-78-3	0.13	106	3	298.9	37.1	531	491	0.92	406	0.76
44	P-78-4	0.23	106	3	298.9	37.1	405	411	1.01	346	0.85
45	P-78-5	0.3	106	3	298.9	37.1	345	354	1.03	308	0.89
46	P-78-6	0.42	106	3	298.9	37.1	256	285	1.11	257	1.00
47	P-78-7	0.57	106	3	298.9	37.1	200	230	1.15	214	1.07
					Huixian et al. [33]						
48		0.07	106	3	299	35.2	603	624	1.03	431	0.71
49		0.14	106	3	299	35.2	531	491	0.92	392	0.74
50		0.24	106	3	299	35.2	405	394	0.97	334	0.82

Table 2. *Cont.*

№	Experiment	e/D_p	D_p, mm	t_p, mm	R_y, MPa	R_b, MPa	N_{exp}, kN	N_1, kN	$\frac{N_1}{N_{exp}}$	N_2, kN	$\frac{N_2}{N_{exp}}$
51		0.32	106	3	299	35.2	345	333	0.97	294	0.85
52		0.45	106	3	299	35.2	255	267	1.05	244	0.96
53		0.6	106	3	299	35.2	200	218	1.09	205	1.03
54		0.1	108.6	4.6	271.9	30.7	674	630	0.93	444	0.66
55		0.15	108.6	4.6	271.9	30.7	612	561	0.92	408	0.67
56		0.2	108.6	4.6	271.9	30.7	551	504	0.91	379	0.69
57		0.25	108.6	4.6	271.9	30.7	431	452	1.05	351	0.81
58		0.3	108.6	4.6	271.9	30.7	433	408	0.94	326	0.75
59		0.33	108.6	4.6	271.9	30.7	445	385	0.87	311	0.70
60		0.35	108.6	4.6	271.9	30.7	433	372	0.86	302	0.70
					Zhong et al. [34]						
61	A1	0.05	108.1	4.21	300.9	21.5	776	754	0.97	547	0.70
62	A2	0.1	103	2	300.9	21.5	285	348	1.22	310	1.09
63	A3	0.15	108	4.21	300.9	21.5	623	505	0.81	385	0.62
64	A4	0.15	108.5	4.75	300.9	21.5	669	551	0.82	409	0.61
65	A5	0.15	103	1.81	300.9	21.5	333	306	0.92	280	0.84
66	A6	0.2	108.1	4.33	300.9	21.5	563	466	0.83	362	0.64
67	A7	0.25	103	4.83	300.9	21.5	314	434	1.38	334	1.06
68	A8	0.25	103.3	2.02	300.9	21.5	289	265	0.92	248	0.86
69	A9	0.3	105.3	3.1	300.9	21.5	353	304	0.86	265	0.75
					Cai et al. [35]						
70	PA2-3	0.06	166	5	277.3	38.2	1642	1589	0.97	1208	0.74
71	PA2-4	0.06	166	5	277.3	38.2	1568	1589	1.01	1208	0.77
72	PA2-5	0.12	166	5	329.3	38.2	1568	1286	0.82	1078	0.69
73	PA2-6	0.12	166	5	294	41.1	1568	1250	0.80	1032	0.66
74	PA2-7	0.18	166	5	286.2	41.1	1127	1079	0.96	896	0.80
75	PA2-8	0.18	166	5	248.9	41.1	1201	1009	0.84	817	0.68
76	PA2-9	0.24	166	5	313.6	38.2	1039	962	0.93	836	0.80
77	PA2-10	0.24	166	5	279.3	38.2	990	902	0.91	763	0.77
78	PA2-11	0.36	166	5	279.3	38.2	735	702	0.96	615	0.84
79	PA2-12	0.36	166	5	296	38.2	843	726	0.86	647	0.77
80	PA2-13	0.6	166	5	296	41.1	564	507	0.90	459	0.81
81	PA2-14	0.6	166	5	296	41.1	510	507	0.99	459	0.90

The second model predicts the maximum load with a safety margin for most samples. The average value of the N_2/N_{exp} ratio is 0.82, the maximum value is 1.11 and the minimum is 0.61. The standard deviation $\sigma = 0.124$ and the coefficient of variation CV = 15.1%. In the design practice, the second model should be used, which takes into account random eccentricities.

Also, the first model, which predicts the values of the ultimate load without taking into account additional random eccentricities, was tested on experimental data for 265 centrally compressed columns, presented in 26 different works [31,36–60]. A comparison of the predicted values with the experimental data is given in Table 3. The diameter of the columns in papers [31,36–60] varied from 100 to 1020 mm, the wall thickness varied from 0.86 to 13.25 mm, the yield strength of steel varied from 165.8 to 853 MPa and the compressive strength of concrete varied from 16.7 to 114.3 MPa.

Table 3. Comparison of ANN predicted values with experimental data for centrally compressed CFST columns.

№	Experiment	D_p, mm	t_p, mm	R_y, MPa	R_b, MPa	N_{exp}, kN	N_1, kN	$\frac{N_1}{N_{exp}}$
				M.H. Lai, J.C.M. Ho [36]				
1	CNO-1-114-30	111.5	0.96	370	31.4	479	513	1.07
2	CNO-1-114-30_1	111.6	0.95	370	31.4	456	513	1.13
3	CNO-1-114-80	111.6	0.96	370	79.9	955	1041	1.09
4	CNO-1-114-80_1	111.8	0.96	370	79.9	979	1043	1.07
5	CNO-3-114-30	114.8	2.86	284.9	31.4	719	709	0.99
6	CNO-3-114-80	114.7	2.86	284.9	79.9	1199	1198	1.00
7	CND-4-139-30_S	139	3.96	289.5	31.7	1010	1073	1.06
8	CN0-4-139-30_R	139	3.97	289.5	30.6	1022	1059	1.04
9	CNO-4-139-50	139	3.99	289.5	51.7	1297	1362	1.05
10	CNO-4-139-100_S	138.7	4	289.5	104.5	2070	1883	0.91
11	CNO-4-139-100_R	139.1	3.94	289.5	101.6	2040	1887	0.93
12	CNO-5-114-50	114.5	4.98	422.6	51.4	1274	1429	1.12
13	CNO-5-114-50_1	114	5.03	422.6	51.4	1379	1430	1.04
14	CNO-5-114-120	114.3	5.01	422.6	114.3	1876	1691	0.90
15	CN0-5-168-30	169.2	4.93	369	29.1	1727	1743	1.01
16	CNO-5-168-60	169.2	5.04	369	61.2	2556	2442	0.96
17	CNO-5-168-80	168.7	4.97	369	85.4	2926	2855	0.98
18	CNO-8-168-30	168.7	7.76	383.6	38.1	2507	2591	1.03
19	CNO-8-168-80	168.2	7.8	361.6	75.2	3101	3181	1.03
20	CNO-10-168-30	168.4	9.91	386.4	27	2533	2879	1.14
21	CNO-10-168-90	168.7	9.96	386.4	95.1	3940	3873	0.98
				Gardner and Jacobson [37]				
22	3	101.7	3.07	650.1	34.1	1112	987	0.89
23	4	101.7	3.07	650.1	31.2	1067	958	0.90
24	8	120.8	4.06	451.6	34.4	1200	1198	1.00
25	9	120.8	4.09	451.6	34.1	1200	1200	1.00
26	10	120.8	4.09	451.6	29.6	1112	1149	1.03
27	13	152.6	3.18	415.1	25.9	1200	1191	0.99
28	14	152.6	3.07	415.1	20.9	1200	1083	0.90
				Luksha and Nesterovich [31]				
29	SB1	530	7.8	349.2	38.3	14,000	13,518	0.97
30	SB2	630	6.6	303	28.4	13,700	13,327	0.97
31	SB3	630	7	225	40	16,200	15,588	0.96
32	SB4	630	7	291.4	40	16,660	16,775	1.01
33	SB5	630	7.61	349.5	38.9	18,000	17,982	1.00
34	SB6	630	7.9	300	40	17,200	17,540	1.02
35	SB7	630	7.9	300	77.8	28,700	28,830	1.00
36	SB8	630	8.44	350	38.3	18,600	18,476	0.99
37	SB9	630	10.21	323.3	42.7	20,500	20,433	1.00
38	SB10	630	11.6	347.2	51.1	24,400	24,500	1.00
39	SB11	720	7.7	395.4	31.4	21,000	20,820	0.99
40	SB12	720	7.93	388.4	37.8	25,500	23,313	0.91
41	SB13	720	8.3	312	16.7	15,000	13,796	0.92
42	SB14	820	8.93	331	50	33,600	34,696	1.03
43	SB15	1020	9.64	336	18.8	30,000	27,689	0.92
44	SB16	1020	13.25	368.7	32.1	46,000	44,305	0.96
				Sakino and Hayashi [38]				
45	L-20-1	178	9	283	21.3	2120	2191	1.03
46	L-20-2	178	9	283	21.3	2060	2191	1.06
47	H-20-1	178	9	283	43.6	2720	2624	0.96
48	H-20-2	178	9	283	43.6	2730	2624	0.96
49	L-32-1	179	5.5	249	21.2	1410	1447	1.03
50	L-32-2	179	5.5	249	22.9	1560	1484	0.95
51	H-32-1	179	5.5	249	42	2080	1898	0.91
52	H-32-2	179	5.5	249	42	2070	1898	0.92
53	L-58-1	174	3	266	22.9	1220	1042	0.85
54	L-58-2	174	3	266	22.9	1220	1042	0.85
55	H-58-1	174	3	266	43.9	1640	1494	0.91
56	H-58-2	174	3	266	43.9	1710	1494	0.87

Table 3. *Cont.*

№	Experiment	D_p, mm	t_p, mm	R_y, MPa	R_b, MPa	N_{exp}, kN	N_1, kN	$\frac{N_1}{N_{exp}}$
				Kato [39]				
57	C04LB	301.5	4.5	381.2	26.6	3851	3758	0.98
58	C06LB	298.5	5.74	399.8	26.6	4537	4361	0.96
59	C08LB	298.4	7.65	384.2	26.6	4919	5046	1.03
60	C12LB	297	11.88	347.9	26.6	5909	6197	1.05
61	C04MB	301.5	4.5	381.2	34.2	4547	4251	0.93
62	C06MB	298.5	5.74	399.8	31	5125	4635	0.90
63	C08MB	298.4	7.65	384.2	34.1	5821	5501	0.95
64	C12MB	297	11.88	347.9	34.2	7222	6632	0.92
65	C2MBH	301.3	11.59	471.4	34.2	8594	8312	0.97
66	C06HB	298.5	5.74	399.8	79.1	7938	7685	0.97
67	C08HB	298.4	7.65	384.2	79.1	8388	8262	0.98
68	C12HB	297	11.88	347.9	79.1	9388	9170	0.98
				Saisho et al. [40]				
69	H-30.1	101.6	2.99	377.3	59.9	921	991	1.08
70	H-30.2	101.6	2.99	377.3	59.9	921	991	1.08
71	H-30.3	101.6	2.96	377.3	59.9	901	987	1.10
72	H-50.1	139.8	2.78	341	55	1323	1330	1.01
73	H-50.2	139.8	2.78	341	55	1391	1330	0.96
74	H-50.3	139.8	2.78	341	55	1313	1330	1.01
75	11-60.1	139.8	2.37	462.6	59.9	1558	1509	0.97
76	H-60.2	139.8	2.37	462.6	68	1577	1648	1.05
77	H-60.3	139.8	2.37	462.6	68	1577	1648	1.05
78	H-60.4	139.8	2.37	462.6	68	1626	1648	1.01
79	L-30.1	101.6	2.96	377.3	24.4	676	658	0.97
80	L-30.2	101.6	2.99	377.3	26.6	715	679	0.95
81	L-30.3	101.6	2.99	377.3	28.2	715	693	0.97
82	L-50.1	139.8	2.78	341	24.4	931	867	0.93
83	L-50.2	139.8	2.78	341	26.6	950	899	0.95
84	L-60.1	139.8	2.37	462.6	26.6	1098	964	0.88
85	L-60.2	139.8	2.37	462.6	26.6	1107	964	0.87
86	L-60.3	139.8	2.37	462.6	26.6	1078	964	0.89
				Yamamoto et al. [41]				
87	C10A-2A-1	101.4	3.02	371	22.3	660	642	0.97
88	C10A-2A-2	101.9	3.07	371	22.3	649	652	1.00
89	C10A-2A-3	101.8	3.05	371	22.3	682	649	0.95
90	C20A-2A	216.4	6.66	452	22.3	3568	3184	0.89
91	C30A-2A	318.3	10.34	331	23.2	6565	5783	0.88
92	C10A-3A-1	101.7	3.04	371	38.6	800	785	0.98
93	C10A-3A-2	101.3	3.03	371	38.6	742	780	1.05
94	C20A-3A	216.4	6.63	452	36.7	4023	3619	0.90
95	C30A-3A	318.3	10.35	339	37.6	7933	6861	0.86
96	C10A-4A-1	101.9	3.04	371	49.2	877	887	1.01
97	C10A-4A-2	101.5	3.05	371	49.2	862	885	1.03
98	C20A-4A	216.4	6.65	452	44.9	4214	3890	0.92
99	C30A-4A	318.5	10.38	339	50.1	8289	7739	0.93
				Schneider [42]				
100	C1	140.8	3	285	28.2	881	891	1.01
101	C2	141.4	6.5	313	23.8	1367	1445	1.06
102	C3	140	6.68	537	28.2	2010	2192	1.09
				O'Shea and Bridge [43]				
103	S30CS50B	165	2.82	363.3	48.3	1662	1611	0.97
104	S20CS50A	190	1.94	256.4	41	1678	1421	0.85
105	S16CS5013	190	1.52	293.1	48.3	1695	1586	0.94
106	S12CS50A	190	1.13	185.7	41	1377	1178	0.86
107	S10CS50A	190	0.86	165.8	41	1350	1108	0.82
108	S30CS80A	165	2.82	363.3	80.2	2295	2260	0.98
109	S20CS80B	190	1.94	256.4	74.7	2592	2300	0.89
110	S16CS80A	190	1.52	293.1	80.2	2602	2427	0.93
111	S12CS80A	190	1.13	185.7	80.2	2295	2139	0.93
112	S10CS80B	190	0.86	165.8	74.7	2451	1933	0.79
113	S30CS10A	165	2.82	363.3	108	2673	2506	0.94

Table 3. *Cont.*

№	Experiment	D_p, mm	t_p, mm	R_y, MPa	R_b, MPa	N_{exp}, kN	N_1, kN	$\frac{N_1}{N_{exp}}$
114	S20CS10A	190	1.94	256.4	108	3360	2813	0.84
115	S16CS10A	190	1.52	293.1	108	3260	2828	0.87
116	S12CS10A	190	1.13	185.7	108	3058	2478	0.81
117	SI10CSI10A	190	0.86	165.8	108	3070	2371	0.77
Elremaily et al. [44]								
118	CU-040	200	5	265.8	27.2	2004	1798	0.90
119	CU-070	280	4	272.6	31.2	3025	2925	0.97
120	CU-150	300	2	244.2	27.2	2608	2261	0.87
Johansson [45]								
121	SFE4	159	5	390	36.6	1770	1812	1.02
122	SFE5	159	6.8	402	36.6	2130	2244	1.05
123	SFE6	159	10	355	36.6	2500	2680	1.07
124	SFE7	159	5	390	93.8	2740	2758	1.01
125	SFE8	159	6.8	402	93.8	3220	3110	0.97
Yu et al. [46]								
126	G4-1a	165	1	222	73.4	1773	1568	0.88
127	G2-2b	151	2	405	69.6	1933	1707	0.88
128	G4-2c	165	2	338	73.4	2077	1927	0.93
129	G4-2d	165	2	338	73.4	1930	1927	1.00
130	G4-2e	165	2	338	73.4	1920	1927	1.00
131	G2-4.5b	151	4.5	438	69.6	2572	2292	0.89
132	G2-6a	159	6	405	69.6	2957	2686	0.91
133	G2-8a	159	8	438	69.6	3173	3235	1.02
134	G2-8b	159	8	438	69.6	3267	3235	0.99
135	G2-8c	159	8	438	69.6	3330	3235	0.97
Giakoumelis and Lam [47]								
136	C3	114.4	3.98	343	25.1	826	863	1.04
137	C4	114.6	3.99	343	78.1	1308	1420	1.09
138	C7	114.9	4.91	365	27.9	1050	1068	1.02
139	C8	115	4.92	365	87.7	1787	1663	0.93
140	C9	115	5.02	365	47.4	1390	1285	0.92
141	C11	114.3	3.75	343	47.4	1013	1060	1.05
142	C12	114.3	3.85	343	25.6	826	848	1.03
143	C14	114.5	3.84	343	82.6	1359	1438	1.06
Gu et al. [48]								
144	0-1.5	127	1.5	350	48.2	890	888	1.00
145	0-2.5	129	2.5	350	48.2	1140	1063	0.93
146	0-3.5	131	3.5	310	48.2	1173	1178	1.00
147	0-4.5	133	4.5	310	48.2	1408	1347	0.96
Han and Yao [49]								
148	scsc1-1	100	3	303.5	48.2	708	780	1.10
149	sch1-1	100	3	303.5	48.2	766	780	1.02
150	scv1-1	100	3	303.5	48.2	780	780	1.00
151	scsc2-1	200	3	303.5	48.2	2320	2083	0.90
152	scsc2-2	200	3	303.5	48.2	2330	2083	0.89
153	sch2-1	200	3	303.5	48.2	2160	2083	0.96
154	sch2-2	200	3	303.5	48.2	2160	2083	0.96
155	scv2-1	200	3	303.5	48.2	2383	2083	0.87
156	scv2-2	200	3	303.5	48.2	2256	2083	0.92
Sakino et al. [50]								
157	CC4-A-2	149	2.96	308	25.4	941	942	1.00
158	CC4-A-8	149	2.96	308	77	1781	1789	1.00
159	CC6-A-2	122	4.54	576	25.4	1509	1409	0.93
160	CC6-A-4-1	122	4.54	576	40.5	1657	1587	0.96
161	CC6-A-4-2	122	4.54	576	40.5	1663	1587	0.95
162	CC6-A-8	122	4.54	576	77	2100	2098	1.00
163	CC6-C-2	239	4.54	507	25.4	3035	3159	1.04
164	CC6-C-4-1	238	4.54	507	40.5	3583	3734	1.04
165	CC6-C-4-2	238	4.54	507	40.5	3647	3734	1.02
166	CC6-C-8	238	4.54	507	77	5578	5218	0.94
167	CC6-D-2	361	4.54	460.7	25.4	5633	5482	0.97
168	CC6-D-4-1	361	4.54	460.7	41.1	7260	6923	0.95
169	CC6-D-4-2	360	4.54	462	41.1	7045	6902	0.98
170	CC6-D-8	360	4.54	462	85.1	11,505	11,056	0.96
171	CC8-A-2	108	6.47	853	25.4	2275	1944	0.85
172	CC8-A-4-1	109	6.47	853	40.5	2446	2161	0.88

Table 3. *Cont.*

№	Experiment	D_p, mm	t_p, mm	R_y, MPa	R_b, MPa	N_{exp}, kN	N_1, kN	$\frac{N_1}{N_{exp}}$
173	CC8-A-4-2	108	6.47	853	40.5	2402	2137	0.89
174	CC8-A-8	108	6.47	853	77	2713	2730	1.01
175	CC8-C-2	222	6.47	843	25.4	4964	5401	1.09
176	CC8-C-4-1	222	6.47	843	40.5	5638	5822	1.03
177	CC8-C-4-2	222	6.47	843	40.5	5714	5822	1.02
178	CC8-C-8	222	6.47	843	77	7304	6972	0.95
179	CC8-D-2	337	6.47	703.3	25.4	8475	8587	1.01
180	CC8-D-4-1	337	6.47	703.3	41.1	9668	9635	1.00
181	CC8-D-4-2	337	6.47	703.3	41.1	9835	9635	0.98
182	CC8-D-8	337	6.47	703.3	85.1	13,776	12,735	0.92
				Zhang and Wang [51]				
183	L-A-1-92h	167.4	3.32	354	39.9	1704	1554	0.91
184	L-A-2-99h	167.3	3.35	354	39.9	1668	1559	0.93
185	L-A-3-98h	167.5	3.33	354	39.9	1700	1558	0.92
186	L-B-1-85h	138.9	3.29	332	34.8	1140	1081	0.95
187	L-B-3-89h	139.5	3.37	332	34.8	1180	1100	0.93
188	L-C-1-87h	139.9	3.58	325	34.8	1222	1128	0.92
189	L-C-2-101h	139.9	3.54	325	34.8	1242	1121	0.90
190	M-A-1-97h	167	3.37	354	56.1	2075	1907	0.92
191	M-A-2-100h	167.1	3.33	354	56.1	2105	1900	0.90
192	M-A-3-95h	167.8	3.33	354	56.1	2055	1912	0.93
193	M-B-1-20h	138.6	3.31	332	49.5	1480	1300	0.88
194	M-C-3-86h	139.7	3.61	325	48.6	1540	1337	0.87
195	M-E-1-21h	133.4	5.17	351	56.1	1810	1655	0.91
196	M-E-2-27h	133.2	5.03	351	56.1	1770	1630	0.92
197	H-B-2-309h	138.7	3.28	332	61.4	1680	1478	0.88
198	H-D-1-311h	159.3	5.36	356	61.4	2480	2261	0.91
199	H-D-2-308h	160.2	5.01	356	61.4	2440	2213	0.91
200	H-F-1-307h	133.3	5.43	392	61.4	1820	1873	1.03
201	H-F-2-313h	133.1	5.44	392	61.4	1915	1871	0.98
				Han et al. [52]				
202	CA2-1	100	1.87	282	70.9	822	834	1.01
203	CA2-2	100	1.87	282	70.9	845	834	0.99
204	CA3-1	150	1.87	282	70.9	1701	1501	0.88
205	CA3-2	150	1.87	282	70.9	1670	1501	0.90
206	CA4-1	200	1.87	282	70.9	2783	2461	0.88
207	CA4-2	200	1.87	282	70.9	2824	2461	0.87
208	CA5-1	250	1.87	274	70.9	3950	3706	0.94
209	CA5-2	250	1.87	274	70.9	4102	3706	0.90
210	CB2-1	100	2	404	70.9	930	982	1.06
211	CB2-2	100	2	404	70.9	920	982	1.07
212	CB3-1	150	2	404	70.9	1870	1711	0.91
213	CB3-2	150	2	404	70.9	1743	1711	0.98
214	CB4-1	200	2	366.3	70.9	3020	2662	0.88
215	CB4-2	200	2	366.3	70.9	3011	2662	0.88
216	CB5-1	250	2	293.1	70.9	4442	3789	0.85
217	CB5-2	250	2	293.1	70.9	4550	3789	0.83
218	CC2-1	150	2	404	75	1980	1783	0.90
219	CC2-2	150	2	404	75	1910	1783	0.93
220	CC3-1	250	2	293.1	75	4720	3974	0.84
221	CC3-2	250	2	293.1	75	4800	3974	0.83
				Tan [53]				
222	GH1-1	125	1	232	97.2	1275	1181	0.93
223	GH1-2	125	1	232	97.2	1239	1181	0.95
224	GH2-1	127	2	258	97.2	1491	1366	0.92
225	GH3-1	133	3.5	352	97.2	1995	1843	0.92
226	GH3-2	133	3.5	352	97.2	1991	1843	0.93
227	GH3-3	133	3.5	352	97.2	1962	1843	0.94
228	GH4-1	133	4.7	352	97.2	2273	2001	0.88
229	GH4-2	133	4.7	352	97.2	2158	2001	0.93
230	GH4-3	133	4.7	352	97.2	2253	2001	0.89
231	GH5-1	127	7	429	97.2	2404	2397	1.00
232	GH5-2	127	7	429	97.2	2370	2397	1.01
233	GH5-3	127	7	429	97.2	2364	2397	1.01

Table 3. *Cont.*

№	Experiment	D_p, mm	t_p, mm	R_y, MPa	R_b, MPa	N_{exp}, kN	N_1, kN	$\frac{N_1}{N_{exp}}$
234	GH6-3	108	4.5	358	88.6	1518	1479	0.97
				Gupta et al. [54]				
235	D4M3C1	112.6	2.89	360	19.8	670	662	0.99
236	D4M3C2	112.6	2.89	360	23	646	693	1.07
237	D4M3C3	112.6	2.89	360	22.4	661	687	1.04
238	D4M4C1	112.6	2.89	360	30.4	786	764	0.97
239	D4M4C2	112.6	2.89	360	32.5	752	786	1.05
240	D4M4C3	112.6	2.89	360	30.6	765	766	1.00
				Yu et al. [55]				
241	SZ3S6A1	165	2.73	350	64.1	2080	1903	0.91
242	SZ3S4A1	165	2.72	350	46.9	1750	1537	0.88
243	SZ3C4A1	165	2.75	350	37.8	1560	1353	0.87
				Lai et al. [56]				
244	F0-102	204	2	226	42.2	1864	1596	0.86
245	F0-135	203	1.5	242	42.1	1699	1509	0.89
246	F0-202	202	1	181.4	35.9	1380	1141	0.83
				Liao et al. [57]				
247	cn-1	180	3.8	360	53	2110	2177	1.03
248	cn-2	180	3.8	360	53	2070	2177	1.05
				Uy et al. [58]				
249	C20-100*1.6A	101.6	1.6	320	20	421	417	0.99
250	C20-100*1.6B	101.6	1.6	320	20	426	417	0.98
251	C30-100*1.6A	101.6	1.6	320	30	477	497	1.04
252	C30-100*1.6B	101.6	1.6	320	30	477	497	1.04
253	C30-150*1.6A	152.4	1.6	279	30	904	792	0.88
254	C30-150*1.6B	152.4	1.6	279	30	890	792	0.89
255	C30-200*2.0A	203.2	2	259	30	1537	1285	0.84
256	C30 200*2.0B	203.2	2	259	30	1550	1285	0.83
				Xue et al. [59]				
257	N3-0-A	219	3	313	51.6	2647	2571	0.97
258	N4-0-A	219	4	313	51.6	2896	2822	0.97
259	N5-0-A	219	5	313	51.6	3218	3066	0.95
				Abed et al. [60]				
260	CFSTf60D167t3.1	167	3.1	300	60	1873	1820	0.97
261	CFSTf60D114t3.6	114	3.6	300	60	1095	1106	1.01
262	CFSTf60D114t5.6	114	5.6	300	60	1297	1338	1.03
263	CFSTf44D167t3.1	167	3.1	300	44	1710	1486	0.87
264	CFSTf44D114t3.6	114	3.6	300	44	1034	938	0.91
265	CFSTf44D114t5.6	114	5.6	300	44	1240	1181	0.95

Despite the fact that some values of the input parameters in Table 3 are outside the range in which the neural network was trained, it showed good ability to extrapolate data. The average value of the ratio N_1 / N_{exp} is 0.96. The maximum value of the ratio N_1 / N_{exp} is 1.14, the minimum is 0.77. The standard deviation $\sigma = 0.06$ and the coefficient of variation CV = 5.9%.

4. Conclusions

During the conducted study, the following main results were obtained:

1. Two models of artificial neural networks have been developed to predict the ultimate load of eccentrically compressed short concrete-filled steel tubular columns of circular cross-sections either without taking into account or taking into account additional random eccentricities. The developed ANNs are based on the theoretical model of the limiting equilibrium of CFST columns. Machine learning models are trained on the entire possible range of the diameters and wall thicknesses of metal tubes, as well as on the wide range of changes in the design strength of concrete and steel. The volume of the training

dataset was 179,025 samples, which is hundreds and thousands of times larger than the sample sizes previously used by other researchers.

2. Training of the ANN models on synthetic data was successful; the trained models are characterized by good performance in terms of mean squared error, and the correlation coefficients between the predicted and target values are close to 1.

3. The results of predicting ultimate loads using artificial neural networks were compared with the results of experiments for 81 eccentrically compressed samples presented in five different works and 265 centrally compressed samples presented in twenty-six papers. The first ANN model, which was trained on ultimate loads determined without taking into account random eccentricities, showed good agreement with experimental data for most samples. The second model, which takes into account random eccentricities in accordance with the requirements of design standards, predicts the maximum load with a safety margin for most prototypes. This model can be used in the design process to quickly determine the bearing capacity of columns at a given eccentricity.

In this work, when training artificial neural networks, the basis was a simplified model for determining the ultimate load, in which the stress diagrams in concrete and steel in the limit state were assumed to be rectangular, and the work of tensile concrete was not taken into account. The goal of our further research will be the development of artificial neural networks based on more complex models [61–63]. In this case, the nonlinearity of the diagrams of concrete and steel, as well as the dilatation effect, will be taken into account. Also, this article considers only short columns, for which the additional eccentricity of the axial force caused by the deflection of the element can be neglected. In the future, it is planned to build ANN models to predict the load-bearing capacity of slender CFST columns.

It should also be noted that artificial neural networks are not the only machine learning algorithm. In some cases, other algorithms turn out to be more effective when applied to concrete and reinforced concrete structures, for example, support vector regression (SVR) [64], multi-objective grasshopper optimization algorithm (MOGOA) [65] and others. In the future, it is also planned by us to use alternative algorithms to analyze the datasets generated in this work.

References

1. Tran, H.; Thai, H.T.; Ngo, T.; Uy, B.; Li, D.; Mo, J. Nonlinear inelastic simulation of high-rise buildings with innovative composite coupling shear walls and CFST columns. *Struct. Des. Tall Spec. Build.* **2021**, *30*, e1883. [CrossRef]
2. Bai, Y.; Wang, J.; Liu, Y.; Lin, X. Thin-walled CFST columns for enhancing seismic collapse performance of high-rise steel frames. *Appl. Sci.* **2017**, *7*, 53. [CrossRef]
3. Kumari, B. Concrete filled steel tubular (CFST) columns in composite structures. *IOSR J. Electr. Electron. Eng.* **2018**, *13*, 11–18.
4. Longarini, N.; Cabras, L.; Zucca, M.; Chapain, S.; Aly, A.M. Structural improvements for tall buildings under wind loads: Comparative study. *Shock Vib.* **2017**, *2017*, 2031248. [CrossRef]
5. Xu, L.; Pan, J.; Yang, X. Mechanical performance of self-stressing CFST columns under uniaxial compression. *J. Build. Eng.* **2021**, *44*, 103366. [CrossRef]

6. Wang, X.; Fan, F.; Lai, J. Strength behavior of circular concrete-filled steel tube stub columns under axial compression: A review. *Constr. Build. Mater.* **2022**, *322*, 126144. [CrossRef]

7. Ilanthalir, A.; Regin, J.J.; Maheswaran, J. Concrete-filled steel tube columns of different cross-sectional shapes under axial compression: A review. *IOP Conf. Ser. Mater. Sci. Eng.* **2020**, *983*, 012007. [CrossRef]

8. Bhatia, S.; Tiwary, A.K. Axial Compression Behavior of Single-Skin and Double-Skin Concrete-Filled Steel Tube Columns: A Review. In *Advances in Construction Materials and Sustainable Environment: Select Proceedings of ICCME 2020*; Springer: Singapore, 2022; pp. 849–861. [CrossRef]

9. Yang, C.; Gao, P.; Wu, X.; Chen, Y.F.; Li, Q.; Li, Z. Practical formula for predicting axial strength of circular-CFST columns considering size effect. *J. Constr. Steel Res.* **2020**, *168*, 105979. [CrossRef]

10. Erdoğan, A.; Güneyisi, E.M.; Süleyman, I.P.E.K. Finite Element Modelling of Ultimate Strength of CFST Column and Its Comparison with Design Codes. *Bilecik Şeyh Edebali Univ. Fen Bilim. Derg.* **2022**, *9*, 324–339. [CrossRef]

11. Ding, F.; Cao, Z.; Lyu, F.; Huang, S.; Hu, M.; Lin, Q. Practical design equations of the axial compressive capacity of circular CFST stub columns based on finite element model analysis incorporating constitutive models for high-strength materials. *Case Stud. Constr. Mater.* **2022**, *16*, e01115. [CrossRef]

12. Nguyen, D.H.; Hong, W.K.; Ko, H.J.; Kim, S.K. Finite element model for the interface between steel and concrete of CFST (concrete-filled steel tube). *Eng. Struct.* **2019**, *185*, 141–158. [CrossRef]

13. İpek, S.; Güneyisi, E.M. Nonlinear finite element analysis of double skin composite columns subjected to axial loading. *Arch. Civ. Mech. Eng.* **2020**, *20*, 9. [CrossRef]

14. Li, B.; Ding, F.; Lu, D.; Lyu, F.; Huang, S.; Cao, Z.; Wang, H. Finite Element Analysis of the Mechanical Properties of Axially Compressed Square High-Strength Concrete-Filled Steel Tube Stub Columns Based on a Constitutive Model for High-Strength Materials. *Materials* **2022**, *15*, 4313. [CrossRef]

15. Hilo, S.J.; Sabih, S.M.; Abdulrazzaq, M.M. Numerical Analysis on the Behavior of Polygonal CFST Composite Columns under Axial Loading Using Finite Element. *J. Eng. Sci. Technol.* **2021**, *16*, 4975–4999.

16. Gupta, A.; Mohan, R.; Bisht, H.; Sharma, A. Experimental testing and numerical modelling of CFST columns under axial compressive load. *Asian J. Civ. Eng.* **2022**, *23*, 415–424. [CrossRef]

17. Isleem, H.F.; Chukka, N.D.K.R.; Bahrami, A.; Oyebisi, S.; Kumar, R.; Qiong, T. Nonlinear finite element and analytical modelling of reinforced concrete filled steel tube columns under axial compression loading. *Results Eng.* **2023**, *19*, 101341. [CrossRef]

18. Tran, V.L.; Thai, D.K.; Kim, S.E. Application of ANN in predicting ACC of SCFST column. *Compos. Struct.* **2019**, *228*, 111332. [CrossRef]

19. Tran, V.L.; Thai, D.K.; Nguyen, D.D. Practical artificial neural network tool for predicting the axial compression capacity of circular concrete-filled steel tube columns with ultra-high-strength concrete. *Thin-Walled Struct.* **2020**, *151*, 106720. [CrossRef]

20. Du, Y.; Chen, Z.; Zhang, C.; Cao, X. Research on axial bearing capacity of rectangular concrete-filled steel tubular columns based on artificial neural networks. *Front. Comput. Sci.* **2017**, *11*, 863–873. [CrossRef]

21. Al-Khaleefi, A.M.; Terro, M.J.; Alex, A.P.; Wang, Y. Prediction of fire resistance of concrete filled tubular steel columns using neural networks. *Fire Saf. J.* **2002**, *37*, 339–352. [CrossRef]

22. Moradi, M.J.; Daneshvar, K.; Ghazi-Nader, D.; Hajiloo, H. The prediction of fire performance of concrete-filled steel tubes (CFST) using artificial neural network. *Thin-Walled Struct.* **2021**, *161*, 107499. [CrossRef]

23. Zarringol, M.; Thai, H.T.; Thai, S.; Patel, V. Application of ANN to the design of CFST columns. *Structures* **2020**, *28*, 2203–2220. [CrossRef]

24. Khan, S.; Ali Khan, M.; Zafar, A.; Javed, M.F.; Aslam, F.; Musarat, M.A.; Vatin, N.I. Predicting the Ultimate Axial Capacity of Uniaxially Loaded CFST Columns Using Multiphysics Artificial Intelligence. *Materials* **2022**, *15*, 39. [CrossRef] [PubMed]

25. Hanoon, A.N.; Al Zand, A.W.; Yaseen, Z.M. Designing new hybrid artificial intelligence model for CFST beam flexural performance prediction. *Eng. Comput.* **2022**, *38*, 3109–3135. [CrossRef]

26. Jiang, H.; Mohammed, A.S.; Kazeroon, R.A.; Sarir, P. Use of the Gene-Expression Programming Equation and FEM for the High-Strength CFST Columns. *Appl. Sci.* **2021**, *11*, 10468. [CrossRef]

27. Vu, Q.V.; Truong, V.H.; Thai, H.T. Machine learning-based prediction of CFST columns using gradient tree boosting algorithm. *Compos. Struct.* **2021**, *259*, 113505. [CrossRef]

28. Hou, C.; Zhou, X.G. Strength prediction of circular CFST columns through advanced machine learning methods. *J. Build. Eng.* **2022**, *51*, 104289. [CrossRef]

29. Zarringol, M.; Thai, H.T. Prediction of the load-shortening curve of CFST columns using ANN-based models. *J. Build. Eng.* **2022**, *51*, 104279. [CrossRef]

30. *SR 266.1325800.2016*; Composite Steel and Concrete Structures. Design Rules. Ministry of Construction of Russia: Moscow, Russia, 2017. Available online: https://meganorm.ru/Data2/1/4293747/4293747659.htm (accessed on 18 December 2023).

31. Luksha, L.K.; Nesterovich, A.P. Strength testing of large-diameter concrete filled steel tubular members. In Proceedings of the Third International Conference on Steel-Concrete Composite Structures, Fukuoka, Japan, 26–29 September 1991; Wakabayashi, M., Ed.; Association for International Cooperation and Research in Steel-Concrete Composite Structures: Bradford, UK, 1991; pp. 67–72.

32. Matsui, C. Slender Concrete Filled Steel Tubular Columns Combined Compressionsnd Bending, Strutural Steel. *Steel-Concert. Compos. Struct.* **1995**, *3*, 29–36.

33. Huixian, T.G.; Ximin, S. Study on the fundamental structural behavior of concrete filled steel tubular columns. *J. Build. Struct.* **1982**, *3*, 13.

34. Zhong, S. Research of confining load of CFST under eccentric loading. *J. Harbin Univ. Civ. Eng. Archit.* **1983**, *3*, 1–18.

35. Cai, Z. Behavior and ultimate strength of short concrete-filled steel tubular columns. *J. Build. Struct.* **1984**, *6*, 13–29.
36. Lai, M.H.A.; Ho, J.C.M. Theoretical axial stress-strain model for circular concrete-filled-steel-tube columns. *Eng. Struct.* **2016**, *25*, 124–143. [CrossRef]
37. Gardner, N.J.; Jacobson, E.R. Structural behavior of concrete-filled steel tubes. *ACI J.* **1967**, *64*, 404–412.
38. Sakino, K.; Hayashi, H. Behavior of concrete filled steel tubular stub columns under concentric loading. In Proceedings of the Third International Conference on Steel-Concrete Composite Structures, Fukuoka, Japan, 26–29 September 1991; pp. 25–30.
39. Kato, B. Compressive strength and deformation capacity of concrete-filled tubular stub columns. *J. Struct. Constr. Eng. AIJ* **1995**, *468*, 183–191. [CrossRef]
40. Saisho, M.; Abe, T.; Nakaya, K. Ultimate bending strength of high-strength concrete filled steel tube column. *J. Struct. Constr. Eng. AIJ* **1999**, *523*, 133–140.
41. Yamamoto, K.; Kawaguchi, J.; Morino, S. Experimental study of the size effect on the behaviour of concrete filled circular steel tube columns under axial compression. *J. Struct. Constr. Eng. AIJ* **2002**, *561*, 237–244. [CrossRef] [PubMed]
42. Schneider, S.P. Axially loaded concrete-filled steel tubes. *J. Struct. Eng.* **1998**, *124*, 1125–1138. [CrossRef]
43. O'Shea, M.D.; Bridge, R.Q. Design of circular thin-walled concrete filled steel tubes. *J. Struct. Eng.* **2000**, *126*, 1295–1303. [CrossRef]
44. Elremaily, A.; Azizinamini, A. Behavior and strength of circular concrete-filled tube columns. *J. Constr. Steel Res.* **2002**, *58*, 1567–1591. [CrossRef]
45. Johansson, M. The efficiency of passive confinement in CFT columns. *Steel Compos. Struct.* **2002**, *2*, 379–396. [CrossRef]
46. Yu, Z.W.; Ding, F.X.; Lin, S. Researches on behavior of high-performance concrete filled tubular steel short columns. *J. Build. Struct.* **2002**, *23*, 41–47.
47. Giakoumelis, G. Axial capacity of circular concrete-filled tube columns. *J. Constr. Steel Res.* **2004**, *60*, 1049–1068. [CrossRef]
48. Gu, W.; Guan, S.W.; Zhao, Y.H.; Cao, H. Experimental study on concentrically-compressed circular concrete filled CFRP-steel composite tubular short columns. *J. Shenyang Arch. Civ. Eng. Inst.* **2004**, *20*, 118–120.
49. Han, L.H.; Yao, G.H. Experimental behaviour of thin-walled hollow structural steel (HSS) columns filled with self-consolidating concrete (SCC). *Thin-Wall Struct.* **2004**, *42*, 1357–1377. [CrossRef]
50. Sakino, K.; Nakahara, H.; Morino, S.; Nishiyama, I. Behavior of centrally loaded concrete-filled steel-tube short columns. *J. Struct. Eng. ASCE* **2004**, *130*, 180–188. [CrossRef]
51. Zhang, S.; Wang, Y.Y. Failure modes of short columns of high-strength concrete filled steel tubes. *China Civ. Eng. J.* **2004**, *37*, 1–10.
52. Han, L.H.; Yao, G.H.; Zhao, X.L. Tests and calculations for hollow structural steel (HSS) stub columns filled with self-consolidating concrete (SCC). *J. Constr. Steel Res.* **2005**, *61*, 1241–1269. [CrossRef]
53. Tan, K.F. Analysis of formulae for calculating loading bearing capacity of steel tubular high strength concrete. *J. Southwest. Univ. Sci. Technol.* **2006**, *21*, 7–10.
54. Gupta, P.K.; Sarda, S.M.; Kumar, M.S. Experimental and computational study of concrete filled steel tubular columns under axial loads. *J. Constr. Steel Res.* **2007**, *63*, 182–193. [CrossRef]
55. Yu, Z.W.; Ding, F.X.; Cai, C.S. Experimental behavior of circular concrete-filled steel tube stub. *J. Constr. Steel Res.* **2007**, *63*, 165–174. [CrossRef]
56. Lai, M.H.; Ho, J.C.M. Confinement effect of ring-confined concrete-filled-steel-tube columns under uniaxial load. *Eng. Struct.* **2014**, *67*, 123–141. [CrossRef]
57. Liao, F.Y.; Han, L.H.; He, S.H. Behavior of CFST short column and beam with initial concrete imperfection: Experiments. *J. Constr. Steel Res.* **2011**, *67*, 1922–1935. [CrossRef]
58. Uy, B.; Tao, Z.; Han, L.H. Behaviour of short and slender concrete-filled stainless steel tubular columns. *J. Constr. Steel Res.* **2011**, *67*, 360–378. [CrossRef]
59. Xue, J.Q.; Briseghella, B.; Chen, B.C. Effects of debonding on circular CFST stub columns. *J. Constr. Steel Res.* **2012**, *69*, 64–76. [CrossRef]
60. Abed, F.; AlHamaydeh, M.; Abdalla, S. Experimental and numerical investigations of the compressive behavior of concrete filled steel tubes (CFSTs). *J. Constr. Steel Res.* **2013**, *80*, 429–439. [CrossRef]
61. Chepurnenko, A.; Yazyev, B.; Meskhi, B.; Beskopylny, A.; Khashkhozhev, K.; Chepurnenko, V. Simplified 2D Finite Element Model for Calculation of the Bearing Capacity of Eccentrically Compressed Concrete-Filled Steel Tubular Columns. *Appl. Sci.* **2021**, *11*, 11645. [CrossRef]
62. Chepurnenko, V.S.; Khashkhozhev, K.N.; Yazyev, S.B.; Avakov, A.A. Improving the calculation of flexible CFST-columns taking into account stresses in the section planes. *Constr. Mater. Prod.* **2021**, *4*, 41–53. [CrossRef]
63. Chepurnenko, A.; Turina, V.; Akopyan, V. Simplified Method for Calculating the Bearing Capacity of Slender Concrete-Filled Steel Tubular Columns. *CivilEng* **2023**, *4*, 1000–1015. [CrossRef]
64. Kandiri, A.; Shakor, P.; Kurda, R.; Deifalla, A.F. Modified Artificial neural networks and support vector regression to predict lateral pressure exerted by fresh concrete on formwork. *Int. J. Concr. Struct. Mater.* **2022**, *16*, 64. [CrossRef]
65. Izadgoshasb, H.; Kandiri, A.; Shakor, P.; Laghi, V.; Gasparini, G. Predicting compressive strength of 3D printed mortar in structural members using machine learning. *Appl. Sci.* **2021**, *11*, 10826. [CrossRef]